Ibn Al-Haitham Journal for Pure and Applied Sciences
Journal homepage: jih.uobaghdad.edu.iq
PISSN: 1609-4042, EISSN: 2521-3407
IHJPAS. 2024, 37(4)

Effect of Adding Al_2O_3 on Some Physical Properties of the Ceramic Compound

Shatha. H. Mahdi[1,*], Saad. K. A[2] and Ulvi Kanbur[3]
[1,2]Department of Physics, College of Education for Pure Sciences (Ibn Al-Haitham), University of Baghdad, Baghdad, Iraq.
[3]Department of Physics, Karabuk University, Karabuk, Türkiye
*Corresponding Author

Received: 30 September 2023 Accepted: 7 June 2023 Published: 20 October 2024
doi.org/10.30536.37.4.3755

Abstract

Zerlokh bentonite is the main material for preparing ceramic specimens with Al_2O_3 additions. X-ray diffraction analyses were carried out on the raw material at room temperature. The specimens of additions that could stand up to 1250 ºC are stable. That is shown by analyzing the X-ray diffraction pattern after heat treatment of the specimens. The growth of new phases like cordierite, anorthite, and cristobalite has the highest percentage ratio of cordierite (76.43%) and mullite (40.28%). So the presence of refractory materials in the obtained samples strongly supports the possibility of using bentonite with additions in the ceramics industry for high temperatures. Therefore, it gave distinct physical and thermal structural properties to the new product. The apparent porosity (A.P.) presented decreases with increasing ratios, and the lowest value for the ratio at 1.5% equals 1%. In studying the thermal conductivity coefficient, the thermal conductivity coefficient increased due to a decrease in ratios. The best values for the thermal conductivity coefficient at 1.5% were (0.045 W/m. °C).

Keywords: Zerlokh Bentonite, mineral, montmorillonite, sedimentation, octahedral shape.

1. Introduction

The clay material consists mainly of small crystallized granules belonging to a limited group of minerals known as clay minerals, where the clay material consists of one mineral and may contain varying amounts of non-clay minerals such as quartz or calcite. Many clay materials include organic materials and salts that solubilize in water. In general, the different clays are aqueous aluminum silicates that contain colloidal materials and quantities of iron and alkaline earth elements, as indicated by chemical analyses. Clay materials are divided into three classes: residual clays, alteration clays, and transported clays [1–5]. Montmorillonite Clay (Bentonite) The name montmorillonite originates from the Montmorillon region in France, and it bears a striking resemblance to mica. However, the bonds between its stratified units are weaker than those in mica due to the entry of water and potassium, a difference in the regular arrangement of these units, and the distribution of the plates, which endows it with a remarkable absorption characteristic [5, 2]. Mineral montmorillonite from the lamellar silicates phylum has the chemical formula [(Ca, Na)12 Mg 2 Al 10 Si24 O60 (OH)].

The crystalline structure of montmorillonite mineral consists of two structural units: a silica tetrahedral sheet resulting from the contact of silicate tetrahedra with each other. Each tetrahedron consists of a silicon atom in its center, surrounded by four oxygen atoms at equal distances, and an alumina octahedral sheet, which consists of two layers of hydroxyl closely packed together. Between the two sheets are aluminum atoms arranged in an octahedral shape [5]. This montmorillonite mineral cell consists of two layers of quaternary silica, between which lies an eight-layer layer of aluminum. The oxygen layers of the quaternary layer form very weak Vander Waals bonds, linking the structural units together. This allows water interlayers and other ions to enter [6–9].

The crystalline structure of bentonite is monoclinic, and its color ranges from white to olive green (gray to greenish-gray) and can be white, yellow, violet, or brown. Its color ranges from white to olive green (gray to greenish-gray), and its density ranges from gm/m3 (2.0-2.7), giving it an opaque or greasy luster [5-8]. The mineral composition of bentonite, which contains a high percentage of montmorillonite, determines its wide range of applications across various industries. This mineral yields various derivatives with diverse chemical and physical properties, making it suitable for many industries. The use of montmorillonite depends on its properties and the mineral composition of Iraqi bentonite. [5,9].

A water-soluble salt like NaCl alters the properties of colloidal bentonite solutions, including viscosity, filtration, and stability. When the NaCl salt concentration is increased, the electrical charge of the colloidal particles decreases. That is, it leads to a decrease in the value of the force of repulsion between the bentonite particles, and thus their merging and the formation of groups that begin with sedimentation [5 9]. The goal of the study is to heat bentonite clay in the Zerlokh region with refractory ceramics (alumina) to a temperature higher than the melting point of regular bentonite (1200 ºC) and then look at the physical properties of the part that is made, such as its mechanical, thermal, and electrical properties.

2. Materials and Methods

2.1. Zerlokh Bentonite.

The Zerlokh region, located in the Diyala Governorate, is known for its bentonite deposits. It is situated 5 km south of the village of Zerlokh and 16 km northwest of the bentonite deposits of the Zerlokh region within the northeastern part of the Hamrin Mountains. The area is dominated by sandstones and some mud, and it is rich in calcium carbonate. Additionally, this region contains two layers that contain montmorillonite minerals. The first layer is the lower one, and its thickness ranges from (0.5–1) m. It is characterized by being rich in this mineral, with a ratio ranging between 50 and 71%. Therefore, this layer is known for its swelling properties. The color of this layer is pale pink-red when dry. The upper layer is located directly above the first layer, as its thickness ranges between (1-4) m. This layer is distinguished by its light weight and contains a small percentage of montmorillonite mineral ranging between 15 and 18%, as well as high percentages of silica and other types of clay. And this layer's color tends to range from gray to white. A thin layer of montmorillonite, ranging in thickness from 7 to 10 cm, covers this deposit, and due to its thinness, it falls within the second layer of the deposit [10]. The Geological Survey Company's tests record the use of bentonite in the Zerlokh region (1).

Table 1. Chemical analysis of Zerlokh Bentonite clay.

SiO_2%	Fe_2O_3 %	Al_2O_3%	TiO_2%	CaO%	MgO%	SO_3%	L.O.I%	Na_2O%	K_2O %
50.6	4.82	15.93	1.69	6.06	4.5	1.06	10. 82	1.25	**0.53**

2.2. Alumina (Al_2O_3)

The alpha phase alumina from the Swiss company (Fluka) was used, with a purity (98%) and a particle size (20 µm).

2.3. The Method of Work.

The materials were mixed using the wet (thermal) mixing method; the value of pH for distilled water was adjusted via litmus paper, where pH = 5,, and then concentrated hydrochloric acid (HCl) was added to the mixture by 2 drops to get a solution with a pH of 2–3. After that, Al_2O_3 was put into ratios of x = 0–1.5% and left to mix for an hour. After that, montmorillonite clay was added to get a dense mixture, and the mixing process continued for 3 hours. The dense mixture was dried by using a laboratory oven at 100 ºC to get rid of the watery solution, then the specimens were formed using the semi-dry pressing method to reduce the porosity arising from the exit of water from the ceramic body during the firing process, and the samples were pressed with a hydraulic press type (RINLNG) of English origin, using a stainless steel mold of 15 mm diameter. To reduce the friction between the walls of the mold and the particles of powder, the mold was lubricated. A force of 7 tons was applied, depending on the research program, and the pressing time was taken at 5 seconds to ensure the smoothness of the measurements. Five samples were formed to conduct tests on them. The heat treatment of the presses was done using an electric furnace (carbolite). The burning was done at normal atmospheric pressure, and the time rate for the temperature rise was 5 ºC/min. The required heat treatment degree is 1250 ºC, and the samples remained at these temperatures for two hours.

2.4. The Tests

2.4.1.Crystal Structure and Microscopic Test

The crystal structure was studied using the X-ray diffraction technique. To characterize the crystal structure of samples of the ceramic material prepared from the samples, the microscopic examination process was carried out using a light microscope of the type of Nikon Eclipse Me600 with Digital Camera DXM1200F with a magnification of 500x.

2.4.2. Apparent Porosity

The Archimedes rule was followed in calculating the apparent porosity according to American specifications [10]. The samples were weighed after sintering while they were dry (Wd) and immersed in water, heated to (100 ºC) for half an hour, left to cool, and then removed from the water After 24 hours, it was weighed again after wiping it with a cotton cloth (Ws). After that, the sample was weighed while immersed in water (Wi) by a system designed for this purpose. The sample was suspended while immersed in water using a metal wire tied at the other end to the sensitive balance at the bottom. Then a calculation was made. apparent porosity of the relationship[11].

$$A.P = \left[\frac{W_s - W_d}{W_s - W_i}\right] \times 100\% \quad (1)$$

W_S: The weight of the sample is wet after immersing it in water, and the open pores are filled. The suspended water droplets on the sample's surface are removed with a clean piece of cloth after being taken out of the water. W_d: dry weight of the sample. W_i: The weight of the model is immersed in water.

2.4.3. Measurement of Thermal Properties.

Measurement of thermal conductivity. To conduct the test, Lee's disc method, as illustrated in **Figure 1**, was followed, where the sample is placed between two plates of lead connected (U, M), also there is a heating coil connected to the battery terminals between the two plates (C, U), at measuring temperatures (Tc, Tu, and Tm) and measuring the thickness of the sample that is in the form of a disk where determent the radius of the disk using the digital micrometer, knowing the electric current of 2.5 amps, the applied voltage of 6 V, and calculating the thermal energy Ht passing through the heating coil, it can be calculated of the thermal conductivity by applying the following equation where two disks were used: of brass, with a diameter of 25 mm, which is almost the same as the diameter of the sample.[12]

$$K\frac{T_U-T_M}{d_s}=h\left[T_M+\frac{2}{r}\left(d_M+\frac{1}{4}d_s\right)T_M+\frac{1}{2r}d_S T_U\right] \quad (2)$$

$$h=\frac{H}{\pi r\left[(T_C-T_M)r+2\left[d_M T_M+\frac{1}{2}d_s(T_M+T_U)+d_U T_U+d_C T_C\right]\right]} \quad (3)$$

I: current flowing (A). V: the applied voltage (volt). T_C, T_U, T_M: disk temperature (C, U, M). r : radius of the disk (mm) . dS: sample thickness. d_U , d_M , d_C : thickness of the discs (C,U,M).

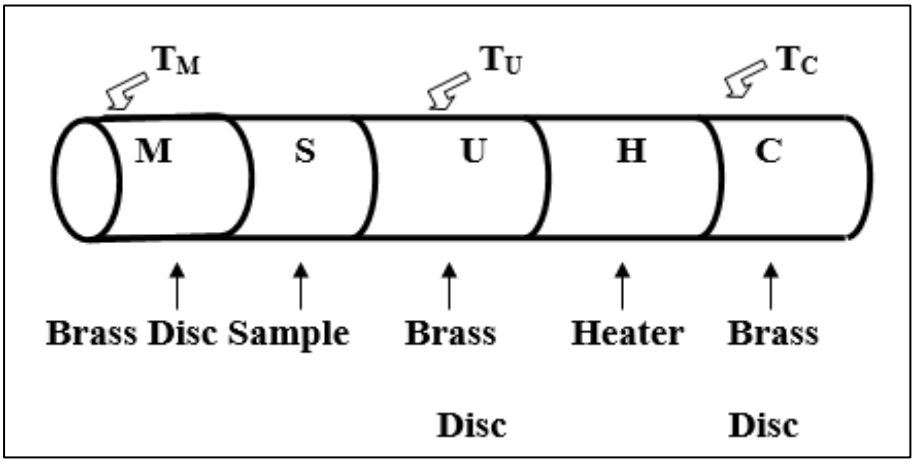

Figure 1. Lee's disc method

3. Results & Discussion

3.1. Structural properties

A group of mineral changes occurred in the raw materials used in ceramic fabrication as a result of disastrous reactions, structural reactions, and the re-formation of new phases [13]. After investigating the XRD patterns shown in **Figures 2** to **5** and balancing them with (2θ) values for all obtained phases with studies pointed to in (ASTM: 39-1425, 15-0776, 21-1152, 12-0301, 12-0303, and 37-1496) cards, estimate the concentrations of those phases [14–18].

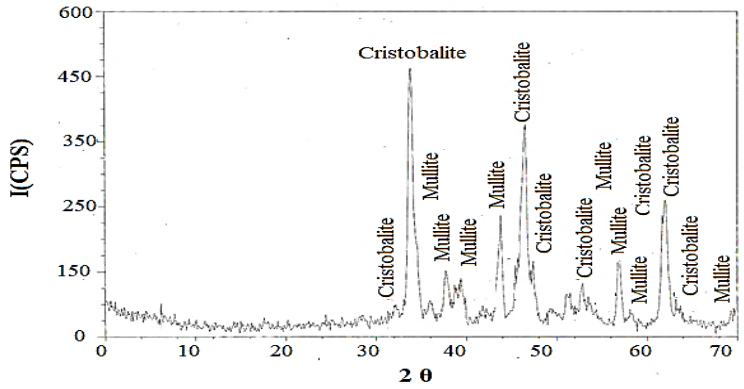

Figure 2. X-ray diffraction patterns of Zerlokh Bentonite, x=0%

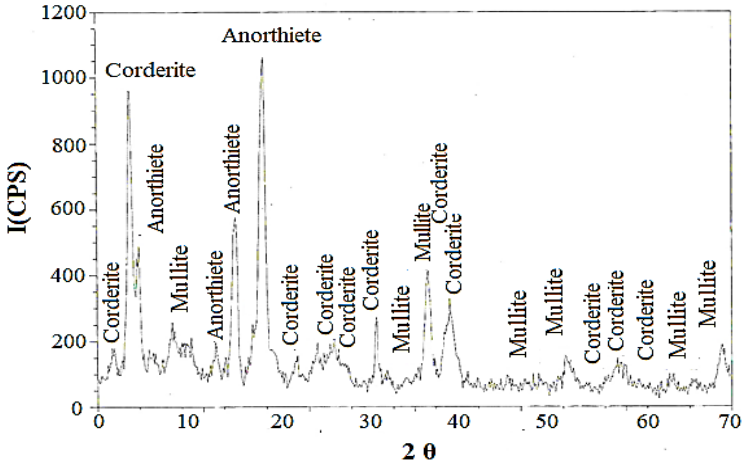

Figure 3. X-ray diffraction patterns at Al_2O_3 additive x=0.5%

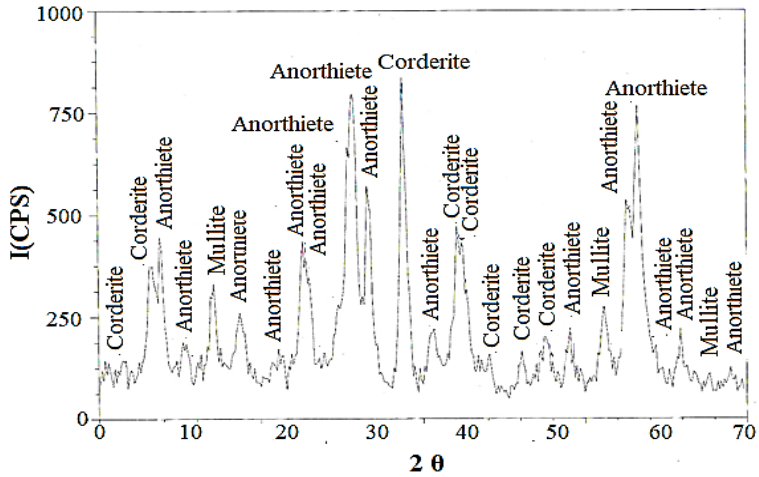

Figure 4. X-ray diffraction patterns at Al_2O_3 additive x=1%

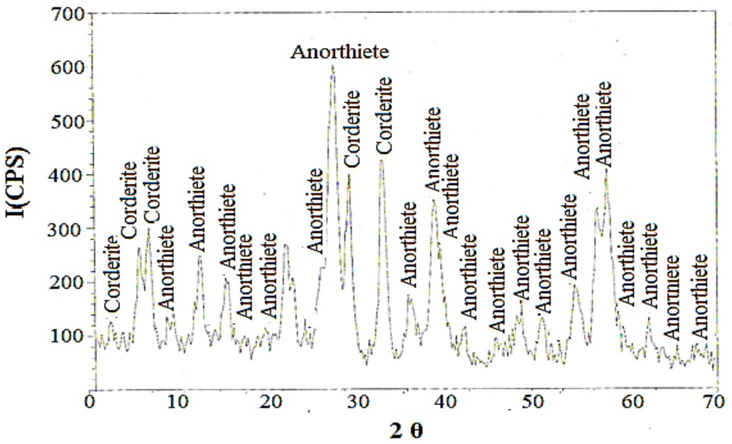

Figure 5. X-ray diffraction patterns at Al_2O_3 additive x=1.5 %

These diagrams refer to the fact that the ceramic samples fabricated from Zerlokh region bentonite, as a base substance with the addition of alumina (Al_2O_3), have been subjected to some mineral changes, the most substantial of which is the disappearance of clay minerals due to their intolerance to high temperatures, which resulted in the fall of their crystalline structure. Also, the calcareous materials break down after they are completely used up, creating other mineral phases. The most important of these are anorthites, cordierite, Cristobalite, and mullite [18–26]. **Table 2** displays the ratios of the resulting new phases. By analyzing the XRD patterns of the treated samples at 1250 ºC within addition ratios, where new phases (Anorthite and Cordierite) appeared in addition to Mullite and Cristobalite, Cordierite was dominant over the rest of the phases, where it can be used in the Electrical insulation industry.

Table 2. The ratios of the resulting new phases.

Samples %	**The ratios of the resulting new phases%**			
	Cristobalite	Mullite	Corderite	**Anorthiete**
0	59.72	40.28	-	**-**
0.5	-	13.52	76.43	**10.05**
1	-	7.62	32.68	**59.70**
1.5	-	-	23.96	**76.04**

3.2. Microscopic examination

Figure 6 shows microscopic images of the surface of the model under the light microscope, and we notice the color of the samples of the material produced from the previous models after being treated with a temperature of 1250 º C and a ripening time of 2 hours. Because of the oxides present in the clay, among these oxides is ferric oxide (Fe^{+3}), which gives a red color, and ferrous oxide (Fe^{+2}), which gives a green or leaden color [27]. When calcium oxide interacts with iron oxide and silica to form new mineral phases [28], it contributes to the white color of the ceramic body and causes a deficiency in the red color caused by iron oxide in the ceramic bodies, transforming it into a yellow color. This interaction results in a deficiency in the red color, and the ceramic samples take on a light brown color. Ceramic samples fired at a temperature of 1250°C exhibit very light yellow and dark yellow colors. The appearance of light brown, green, and reddish-green colors on the ceramic samples indicates the presence of iron oxide, which is a pigment that coats the granules or granules of iron oxide minerals.

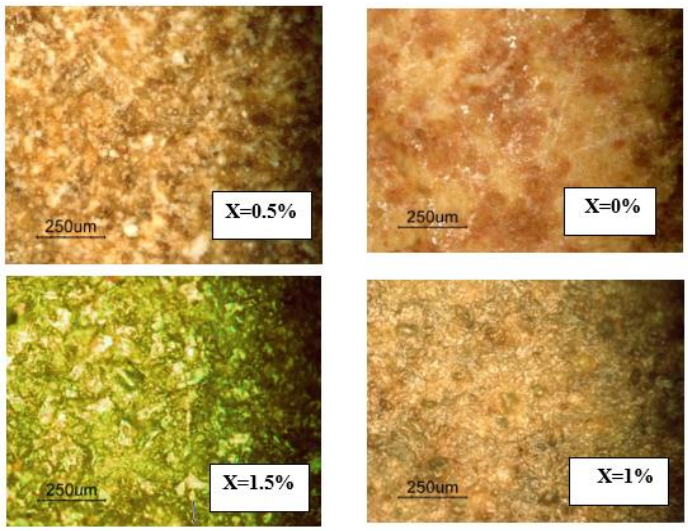

Figures 6. Microscopic images of the surface at x= 0 to 1.5

3.3. Apparent Porosity

Firing losses (L.O.I.), which result in calcium oxide and carbon dioxide and cause the presence of gaps, channels, and connections between the gaps, affect the porosity of the produced ceramic body. The quality of the raw materials used in the preparation of the ceramic body affects porosity. The finer the grain size, the faster the burning process. As shown in **Figure 7**, the amount of pressure used during the model pressing process also changes the porosity of the body. At a temperature of 1250 ºC, the apparent porosity value of the fired models goes down. This causes the granules to converge with each other and block the pores, resulting in a reduction in the apparent porosity values of the produced ceramic body [29].

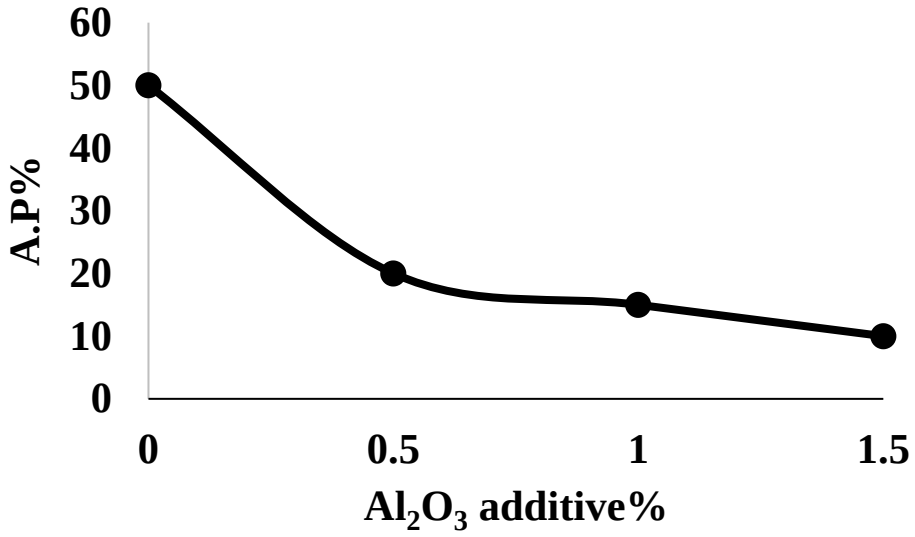

Figures 7. Apparent porosity of samples with Al_2O_3 additive , x= 0 to 1.5 %

3.4. Thermal Conductivity

Observing the results, the thermal conductivity increases, as shown in **Figure 8**, and this is due to the increase in the rates of phase transitions, which are characterized by their relatively high ability to increase the thermal conductivity (the glass phase) because of their treatment at a

temperature of 1250 ºC. This decrease in porosity led to an increase in the thermal storage capacity, which in turn led to a decrease in the thermal insulation capacity because of the decrease in the proportion of air entering the pores, which is characterized by low thermal conductivity [30,31].

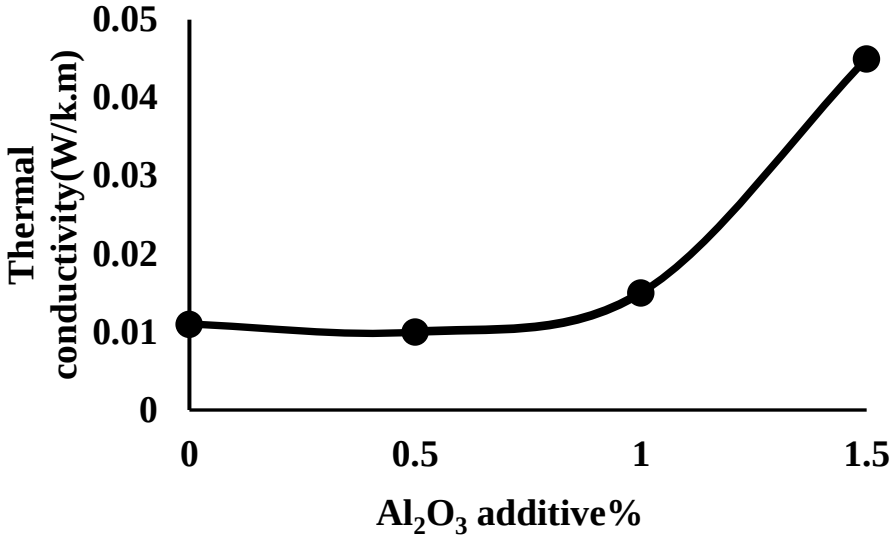

Figures 8. thermal conductivity of samples with Al_2O_3 additive , x= 0 to 1.5

4. Conclusion

Based on the achieved results and their discussion, which show the manufacturing conditions and the nature of the raw materials used in the fabrication of ceramic models, the following conclusions were reached: We were able to create a ceramic model of Zerlokh bentonite using limited ratios of Al2O3, which could withstand a temperature of up to 1250°C. The addition of Al_2O_3 led to the formation of two main phases that gave distinct structural and thermal insulation properties to the new product. We noticed that the apparent porosity decreased with the increase in the percentage of alumina addition, as it was the lowest value of porosity at 1.5%. The best thermal conductivity is at 1.2%.

Acknowledgment

I would like to express my heartfelt gratitude to the University of Baghdad, the College of Education for Pure Science, Ibn Al-Haitham, and the Department of Physics staff for their support. for providing analysis tests.

Conflict of Interest

The authors declare that they have no conflicts of interest.

Funding

None.

References

1. Kareem, A.J.; Mohammed, A.T.; Ebtisam, M.T.; Shatha, H.M. Study characteristics of (epoxy–bentonite doped) composite materials. *Energy Procedia* **2017**, *119*, 670-679. https://doi.org/10.1016/j.egypro.2017.07.094
2. Maryam, M. Bentonite Clay As A Natural Remedy. *A Brief Review Iran J Public Health* **2017**, 46(*9*), 1176-1183. https://doi.org/j.1029026782/100.23

3. Tole, I.; Habermehl, K.; Cwirzen, A. Mechanochemical activation of natural clay minerals: an alternative to produce sustainable cementitious binders. *review, Mineral. Mineralogy and Petrology* **2019**, *113*, 449-462. https://doi.org/10.1007/s00710-019-00666-y
4. Athraa, N.A.; Shatha, H.M. The effect of heat treatment on structure property of (Bentonite-Alumina-Silica) Ceramic. *J. Phys.: Conf. Ser*. **2021**, *1879*, 032119. https://doi:10.1088/1742-6596/1879/3/032119
5. Shatha, H.M.; Ahmed, F.M.; Mohammad, H.M. Effect of gamma radiation on Structural characteristic of Ceramic body, *Mesop. environ. j. Special Issue C* **2017**, 87-90.
6. Ahmed, Z. K.; Özlem C.; Yiannis, P.; Andrew, H.; Pascaline, P.; Susan, A.; Bernal, A.; Marsh, T.M. Advances in alkali-activation of clay minerals. *Cement and Concrete Research* **2020**, *132*, 106050. https://doi.org/10.1016 /j.cemconres.2020.106050
7. Zhang, W.W.; Yunliang, Z.; Haoyu, B.; Tong, W.; Shichang, K.; Guangsen, S.; Sridhar, K. Removal of heavy metals and dyes by clay-based adsorbents: From natural clays to 1D and 2D nano-composites. *Chemical Engineering Journal* **2021**, *420*(*2*), 15, 127574. https://doi.org/10. 1016/j.cej.2020.127574
8. Uma, S.M.; Muthukumar, M. Comprehensive review of geosynthetic clay liner and compacted clay liner, *IOP Conf. Series: Materials Science and Engineering* **2017,** *263*, 032026. https://doi:10.1088/1757-899X/263/3/032026
9. Aref, A.; Hongping, H.; Jianxi, Z.; Yunfei, Xi.; Runliang, Z.; Lingya, M.; Qi, T. Adsorption of ammonium by different natural clay minerals: characterization, kinetics and adsorption isotherms *Appl. Clay Sci*. **2018**, *159*, 83-93. https://doi.org/10.1016/j.clay.2017.11.007
10. Lenz, F.; Birkenstock, J.; Fischer, L.A.; Schneider, H.; Fischer, R.X. Mullite-2c – a natural polytype of mullite. *European Journal of Mineralogy* **2020**, *32*, 235-249. https://doi. org/10.5194/ejm-32-235-2020
11. Szuszkiewicz Astm, C. R23 Standard Test Methods for Determination of Water Absorption and Associated Properties by Vacuum Method for Pressed Ceramic Tiles and Glass Tiles and Boil Method for Extruded Ceramic Tiles and Non-tile Fired Ceramic Whiteware. *Appl. Phys*. **2018,** *21(2)*, 23-34.
12. Astm, C. Standard Test Methods for Apparent Porosity, Water Absorption, Apparent Specific Gravity, and Bulk Density of Burned Refractory Brick and Shapes by Boiling Water. *Appl. Phys*. **2022,** *11(12)*, 43-64.
13. Neamah, Z.J.; Mahdi, S.H.; Effect of zirconia addition on thermal and mechanical properties of poly-methyl methacrylate composites. *Digest Journal of Nanomaterials and Biostructures* **2023**, *18*, 927-932. https://doi.org/10. 15251/DJNB.2023.183.927
14. Lazaratou, C.V.; Vayenas, D.V.; Papoulis, D. The role of clays, clay minerals and clay-based materials for nitrate removal from water systems: *A review Applied Clay Science* **2020** *185*, 105377. https://doi.org/10.1016/j.clay. 2019.105377
15. Ken, L. X-ray Diffraction, A program to analyze energy and angular dispersive, X-ray diffraction patterns. *Appl. Phys*. **1992,** *5(2)*, 45-56.
16. Astm, A. International Center for Diffraction Data, File™ & Related Products. *Jour. Phys.* **2009,** *2(11)*, 33-45.
17. Yasushi, S.; Norihiko, K. Quantitative Analysis Of Tridymite And Cristobalite Crystallized In Rice Husk Ash By Heating. *Industrial Health* **2004**, *42*, 277–285
18. Laurence N.W. Recommended abbreviations for the names of clay minerals and associated phases, *Clay Minerals* **2020**, *55*, 261–264. https://doi:10.1180/clm.2020.30
19. Lenz, S.; Birkenstock, J.; Fischer, L.A.; Schüller, W.; Schneider, H.; Fischer, R.X. Natural mullites: chemical composition, crystal structure, and optical properties. *Eur. J. Mineral*. **2019**, *31*, 353–367, https://doi.org/10.1127/ejm/2019/0031-2812
20. Igami, Y.; Ohi, S.; Kogiso, T.; Furukawa, N.; Miyake, A. High-temperature structural change and microtexture formation of sillimanite and its phase relation with mullite, *American Mineralogist: Journal of Earth and Planetary Materials* **2019**, *104(7)*, 1051-1061. https://doi.org/10.2138/am-2019-6732

21. Szuszkiewicz, A.; Pieczka, A.; Gadas., P.; Vašinová, M.; Szełęg, E.; Gołębiowska, B.; Galusková, D. First occurrence of Mn-dominant cordierite-group mineral: Electron microprobe and laser ablation ICP-MS study. *The Canadian Mineralogist*, **2019**, *57*, 807-810.
22. Zdeněk, K.; Marta, V.; Lucie, B.; Petra, M. Quantitative Evaluation of Crystalline and Amorphous Phases in Clay-Based Cordierite Ceramic. *Minerals* **2020**, *10(12)*, 122. https://doi.org/10.3390/min10121122
23. Valášková, M.; Klika, Z.; Novosad, B.; Smetana, B. Crystallization and quantification of crystalline and non-crystalline phases in kaolin-based cordierites. *Materials* **2019**, *12(19)*, 3104
24. Jin, S.; Xu, H.; Wang, X.; Jacobs, R.; Morgan, D. The incommensurately modulated structures of low-temperature labradorite feldspars: a single-crystal X-ray and neutron diffraction study. *Acta Crystallographica* **2020**, *76*, 93-107.
25. Götz, E.; Kleebe, H.; Kolb, U. The hierarchical internal structure of labradorite, *European Journal of Mineralogy* **2022**, *34*, 393-410.
26. Sokol'skii, V.E.; pruttskov, D.V.; yakovenko, O.M.; Kazimirov, V.P.; Roik, O.S.; Golovataya, N.V.; Sokolsky. G.V. X-rayDiffraction Study Of Structure Of CaO- Al_2O_3-SiO_2 Ternary Compounds In Molten And Crystalline State *J. Min. Metall. Sect. B-Metall* **2020**, *56*, 269 – 277. https://doi.org/10.2298/JMMB190806016S
27. Shigeru, S. Characterization of Formation of Ferrous and Ferric Oxides in Aqueous Solution from a Multidisciplinary Viewpoint. *ISIJ International* **2022** , *62* , 800-810. https://doi.org/10.2355/isijinternational ISIJINT-2021-027
28. Kamil, G.G. Diversity of Iron Oxides: Mechanisms of Formation, Physical Properties and Applications. *Magnetochemistry* **2023**, *9*, 119. https://doi.org/10.3390/magnetoch emistry9050119
29. Ezzat, A.E.; Anwar, S.A.; Mobarak, H.A.; Doreya, M.I. Rheological, physico-mechanical and microstructural properties of porous mullite ceramic based on environmental wastes. *Boletín de la Sociedad Española de Cerámica y Vidrio* **2022**, *61*, 121-129. https://doi.org/10.1016/j.bsecv.2020.08.002
30. Pia, G.; Casnedi, L.; Sanna, U. Porosity and pore size distribution influence on thermal conductivity of yttria-stabilized zirconia: experimental findings and model. *predictions Ceram Int.* **2016,** *42*, 5802-5809. https://doi.org/10.1016/j.ceramint.2015.12.122
31. AbdoulRazac, S.; Doan, P.; Nawal. S.; Rachid, B.; Claudia, T.; Alain, G.; Ange, N. Clay/phosphate-based ceramic materials for thermal energy storage – Part I: Effect of synthetic phosphate content on microstructure, thermo-physical and thermo-mechanical properties. *Open Ceramics* **2023,** *14*, 100346. https://doi.org/10.1016/j.oceram. 2023.100346.